Order online now!

www.rockland.com
tech@rockland.com
+1 484.791.3823

Datasheet for 600-401-C49

ATG13 phospho S318 Antibody

Overview

Description:	Anti-ATG13 pS318 (RABBIT) Antibody - 600-401-C49
Item No.:	600-401-C49
Size:	100 µg
Applications:	Dot Blot, ELISA, WB, FC, IF, Multiplex
Reactivity:	Human
Host Species:	Rabbit

Product Details

Background:	ATG13 is a target of the TOR kinase signaling pathway that regulates autophagy through the control of the phosphorylation status of ATG13 and ULK1 through their stable complex, and the regulation of ATG13-ULK1-RB1CC1. ATG13 also forms a stable complex with FIP200. Ulk1 phosphorylates ATG13 on S318 and promotes its release to damaged mitochondria. Autophagy is a normal process in eukaryotes required for turnover of cellular components during starvation and stress. It plays an essential role in cellular differentiation, cell death and aging. Defects in this evolutionarily conserved process may contribute to certain human diseases such as cancer, neurodegenerative diseases, muscular disorders and pathogen infections. ATG13 is one of several ATG genes required for autophagosome formation in mammalian cells. mTOR interacts with this complex in a nutrient dependent manner and phosphorylates Atg13 and ULK1.
Synonyms:	rabbit anti-ATG13 pS318 Antibody, ATG-13, ATG 13, Autophagy-related protein 13, KIAA0652
Host Species:	Rabbit
Clonality:	Polyclonal
Format:	IgG

Target Details

Gene Name:	ATG13
Reactivity:	Human
PTM Specificity:	Phosphorylation

Immunogen Type:	Conjugated Peptide
Immunogen:	Anti-ATG13 pS318 antibody was prepared by repeated immunizations with a synthetic phospho-peptide corresponding to the region near S318 of ATG13.
Purity/Specificity:	This affinity-purified antibody is directed against the phosphorylated form of human ATG13 protein at the pS318 residue. The product was affinity purified from monospecific antiserum by immunoaffinity purification. Antiserum was first purified against the phosphorylated form of the immunizing peptide. The resultant affinity purified antibody was then cross adsorbed against the non-phosphorylated form of the immunizing peptide. Reactivity occurs against human ATG13 pS318 protein and the antibody is specific for the phosphorylated form of the protein. Reactivity with non-phosphorylated human ATG13 is minimal by ELISA and western blot. A BLAST analysis was used to suggest cross reactivity with ATG13 from human based on 100% sequence homology with the immunogen. Reactivity against homologues from other sources is not known.
Relevant Links:	• UniProtKB - O75143 • NCBI - NP_001136145.1 • GeneID - 9776

Application Details

Tested Applications:	Dot Blot, ELISA, WB
Suggested Applications:	FC, IF, Multiplex (Based on references)
Application Note:	This affinity purified antibody has been tested for use in ELISA and by western blot. Specific conditions for reactivity should be optimized by the end user. Expect a band approximately 56.6 kDa in size corresponding to human phosphorylated ATG13 protein by western blotting in the appropriate stimulated tissue or cell lysate or extract.
Assay Dilutions:	All assays should be optimized by the user. Recommended dilutions (if any) may be listed below.
ELISA:	1:25,000-1:175,000
FC:	User Optimized
WB:	1:2000

Formulation

Physical State:	Liquid (sterile filtered)
Concentration:	1.2 by UV absorbance at 280 nm
Buffer:	0.02 M Potassium Phosphate, 0.15 M Sodium Chloride, pH 7.2

Preservative:	0.01% (w/v) Sodium Azide
Stabilizer:	None

Shipping & Handling

Shipping Condition:	Dry Ice
Storage Condition:	Store vial at -20° C prior to opening. Aliquot contents and freeze at -20° C or below for extended storage. Avoid cycles of freezing and thawing. Centrifuge product if not completely clear after standing at room temperature. This product is stable for several weeks at 4° C as an undiluted liquid. Dilute only prior to immediate use.
Expiration:	Expiration date is one (1) year from date of receipt.

Images

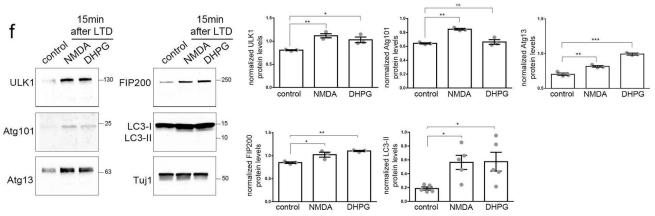

Western Blot
Autophagic vesicles are locally formed in dendrites of cultured neurons following LTD. A) Top, representative super-resolution microscopy dSTORM image of a secondary dendrite labeled with an antibody against LC3, 15 min after cLTD. Bottom, magnification of representative U-shaped LC3-positive structures in dendrites, 15 min after NMDA or DHPG pulses. Scale bars: 2 µm and 250 nm, as indicated. (N = 3 independent experiments). B) Graph showing the number of LC3-positive U-shaped structures in secondary dendrites visualized in (a), before (control) and 15 min or 60 min after NMDAR- and mGluR-LTD. Bars represent mean values ± SEM. N = 3 independent experiments per condition (n > 9 dendrites per condition). Statistical analysis was performed by one-way ANOVA. For the time point of 15 min $F(2, 33) = 17.93$, $p < 0.0001$) (Tukey's test Pcontrol-NMDA < 0.0001, Pcontrol-DHPG < 0.0001). For the time point of 60 min $F(2, 21) = 9.459$, $p = 0.0012$) (Tukey's test Pcontrol-NMDA = 0.0041, Pcontrol-DHPG = 0.0024). C) Graph showing the size distribution (nm) of the dendritic U-shaped LC3-positive structures visualized in a upon NMDAR- and mGluR-LTD. Bars represent mean values ± SEM for each analysed dendrite. N = 3 independent experiments (n > 40 dendrites per condition). D) Confocal images of dendrites immunolabeled with antibodies against WIPI2, LC3, and MAP2 before (control) or after 15 min of NMDAR- and mGluR-LTD. Scale bar: 10 µm. (N = 6 independent experiments). E) Representative confocal images of neurons immunolabeled with antibodies against ULK1, Atg101,

Atg13, FIP200 and, along with MAP2 to label dendrites before (control) or 15 min after LTD-inducing pulses. Scale bar: 20 µm. Graphs showing the number of puncta positive for each ULK1-complex component in secondary dendrites, normalized for dendrite length, in every condition, as indicated. Graph bars represent mean values ± SEM. N = 6 independent experiments per condition. Statistical analyses were performed using one-way ANOVA. ULK1: $F(2,15) = 24.48$, $P < 0.0001$ (Tukey's multiple comparison test, Pcontrol_NMDAR < 0.0001, Pcontrol_mGluR < 0.0001, PNMDAR_mGluR = 0.8825). Atg101: $F(2,15) = 24.31$, $P < 0.0001$ (Tukey's multiple comparison test, Pcontrol_NMDAR < 0.0001, Pcontrol_mGluR < 0.0001, PNMDAR_mGluR = 0.9329). Atg13: $F(2,15) = 8.386$, $P = 0.0036$ (Tukey's multiple comparison test, Pcontrol_NMDAR = 0.007, Pcontrol_mGluR = 0.0086, PNMDAR_mGluR = 0.9940). FIP200: $F(2,15) = 17.66$, $P = 0.0001$ (Tukey's multiple comparison test, Pcontrol_NMDAR = 0.0002, Pcontrol_mGluR = 0.0009, PNMDAR_mGluR = 0.6440). F) Western blot analyses for Atg13, FIP200, ULK1, Atg101, LC3, and β-III tubulin (Tuj1) in neuronal lysates, under control conditions and 15 min after NMDAR- and mGluR-LTD. Graphs showing the normalized protein levels of Atg13, FIP200, ULK1, Atg101 under the aforementioned conditions. Bars represent mean values ± SEM. N = 3 independent experiments for ULK1 complex proteins, N = 5 independent experiments for LC3-II. Statistical analyses were performed using one-way ANOVA. ULK1: $F(2,6) = 13.57$, $P = 0.0059$ (Tukey's multiple comparison test Pcontrol_NMDA = 0.0056, Pcontrol_DHPG = 0.0253). Atg101: $F(2,6) = 27.57$, $P = 0.0009$ (Tukey's multiple comparison test Pcontrol_NMDA = 0.0013, Pcontrol_DHPG = 0.79). Atg13: $F(2,6) = 113.1$, $P < 0.0001$ (Tukey's multiple comparison test Pcontrol_NMDA = 0.0027, Pcontrol_DHPG < 0.0001). FIP200: $F(2,6) = 15.14$, $P = 0.0045$ (Tukey's multiple comparison test Pcontrol_NMDA = 0.0240, Pcontrol_DHPG = 0.041). LC3-II: $F(2, 12) = 4,969$, $P = 0.0268$ (Tukey's multiple comparison test Pcontrol_NMDA = 0.0478, Pcontrol_DHPG = 0.0421). Figure provided by CiteAb. Source: Nat Commun, PMID: 35115539.

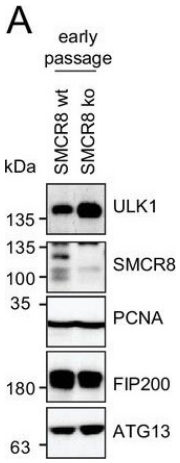

Western Blot

Restored regulation of ULK1 protein levels in SMCR8 knockout cells.(A,B) Early (A) or late (B) passages of HAP1 SMCR8 wildtype (wt) or knockout (ko) cells were subjected to SDS-PAGE and immunoblot with indicated antibodies. PCNA served as loading control. (C) 293T SMCR8 wildtype (wt) or knockout (ko) cells were analyzed as in (A). (D) 293 T cells were transfected with non-targeting control (sicon) or SMCR8 siRNA. Half of the cells were re-transfected every 2–3 days with non-targeting control (sicon) or SMCR8 siRNA while the other half was harvested and subjected to SDS-PAGE and immunoblotting with indicated antibodies. PCNA served as loading control.DOI:http://dx.doi.org/10.7554/eLife.23063.027 Figure provided by CiteAb. Source: Elife, PMID: 28195531.

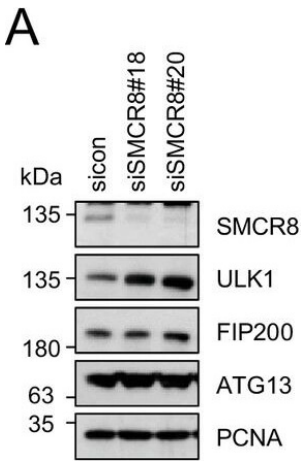

Western Blot

SMCR8 regulates ULK1 gene expression.(A) Lysates from 293 T cells transfected with non-targeting control (sicon) or SMCR8 siRNA were subjected to SDS-PAGE and immunoblotting with indicated antibodies. PCNA served as loading control. (B) Lysates from 293 T cells transfected with non-targeting control (sicon) or SMCR8 siRNA as well as with HA-tagged SMCR8 were subjected to SDS-PAGE and immunoblotting with indicated antibodies. PCNA served as loading control. exp. = exposure. (C) Lysates from 293 T cells transfected with indicated siRNAs and grown in absence (DMSO) or presence of 250 nM Torin1 for 2 hr were lysed and analyzed as in (A). Vinculin served as loading control. (D,E) 293T (D) or U2OS (E) cells were transfected with indicated siRNAs for 72 hr prior to RNA isolation, preparation of cDNA and RT-qPCR with ULK1, FIP200 and SMCR8 specific primers. Error bars represent SEM. Significance was determined using two-way ANOVA compared with sicon. All experiments were performed n = 3.DOI:http://dx.doi.org/10.7554/eLife.23063.026 Restored regulation of ULK1 protein levels in SMCR8 knockout cells.(A,B) Early (A) or late (B) passages of HAP1 SMCR8 wildtype (wt) or knockout (ko) cells were subjected to SDS-PAGE and immunoblot with indicated antibodies. PCNA served as loading control. (C) 293T SMCR8 wildtype (wt) or knockout (ko) cells were analyzed as in (A). (D) 293 T cells were transfected with non-targeting control (sicon) or SMCR8 siRNA. Half of the cells were re-transfected every 2–3 days with non-targeting control (sicon) or SMCR8 siRNA while the other half was harvested and subjected to SDS-PAGE and immunoblotting with indicated antibodies. PCNA served as loading control.DOI:http://dx.doi.org/10.7554/eLife.23063.027 Figure provided by CiteAb. Source: Elife, PMID: 28195531.

Western Blot

Inhibition of Autophagy Flux at Lysosomal Level and Decrease in Autophagy Initiation Signaling in DRPLA(A–C) The ratio of LC3II to LC3I was used to quantify autophagic flux in western blot analysis of full-length GFP-LC3 in the supernatant fraction of cerebellar lysates at 14 weeks of age (A). The anti-LC3 antibody recognizes a doublet between 35 and 55 kDa (Figure S4B), consistent with GFP-LC3-I (upper) and cleaved GFP-LC3-II (lower). The level of Atg5-12 conjugate was used to quantify the events of autophagy initiation. Densitometric analysis shows a decreased relative

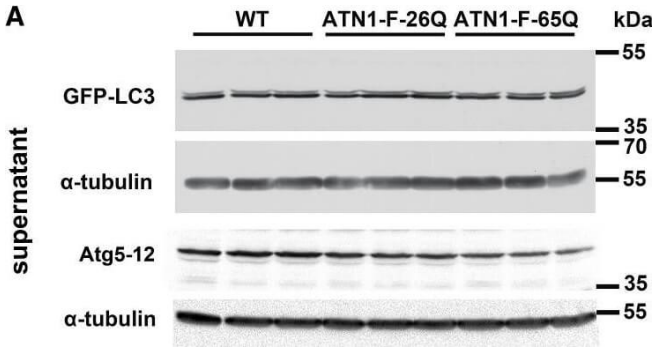

abundance of cleaved GFP-LC3-II to full-length GFP-LC3-I (B) in ATN1-FL-65Q;GFP-LC3 (65Q) mice compared to ATN1-FL-26Q;GFP-LC3 (26Q) and WT;GFP-LC3 (wt) mice. Atg5-12 conjugate (C) is also decreased in ATN1-FL-65Q;GFP-LC3 (65Q) compared to WT;GFP-LC3 (wt). Student's t test, mean ± SEM, ??p < 0.01, ?p < 0.05.(D–F) The accumulation of GFP cleavage product and autophagy receptor p62 was analyzed as a measure of autophagy flux blockage in western blot assay of the cerebellar lysates at 14 weeks of age (D). Mouse anti-GFP antibody recognizes only GFP-LC3-II (Figure S4B) and cleaved GFP after longer exposure. ?Shorter exposure of anti-GFP signal. Densitometric analysis of the relative abundance of cleaved GFP to GFP-LC3-II (E) as well as the abundance of p62 relative to α-tubulin (F) in WT;GFP-LC3 mice (wt), ATN1-FL-26Q;GFP-LC3 (26Q) and ATN1-FL-65Q;GFP-LC3 (65Q) mice. Student's t test, mean ± SEM, ?p < 0.05.(G) Accordingly, western blot analysis of autophagy shows a stall in autophagy flux in end-stage ATN1-FL-65Q mice compared to wild-type (WT) as evidenced by relative decrease of GFP-LC3-II as well as increase of p62 in the pellet fraction. ?Anti-p62 antibody revealed an additional band 20 kDa above the expected band at around ?60 kDa in the supernatant fractions of the cerebellum in end-stage mice.(H) qPCR analysis of Tfeb mRNA levels in the cerebellum of wild-type (wt, white), ATN1-FL-26Q (26Q, blue) and ATN1-FL-65Q mice (65Q, red) at presymptomatic (3 weeks) and early symptomatic (10 weeks) time points. Relative levels normalized to β-actin and Hprt1 are given as a fold change of wild-type. Two-way ANOVA, v1, genotype; v2, age, mean ± SEM (n = 6), ???p < 0.001.(I and J) Levels of Tfeb protein in the supernatant fraction of cerebellar lysates at 14 weeks of age (I). Densitometric analysis (J) reveals a significant decrease in ATN1-FL-65Q;GFP-LC3 (65Q) compared to WT;GFP-LC3 (wt). One-way ANOVA, mean ± SEM, ??p < 0.05.(K) qPCR analysis of Ctsb and Prkag mRNA levels in the cerebellum of wild-type (wt, white), ATN1-FL-26Q (26Q, blue) and ATN1-FL-65Q mice (65Q, red) at an early symptomatic (10 weeks) time point. Relative levels normalized to Hprt1 are given as a fold change of wild-type. One-way ANOVA, mean ± SEM (n = 6), ?p < 0.05, ??p < 0.01, ???p < 0.001.(L) Whole-cell lysates of human fibroblasts from healthy control and DRPLA patients were subjected to western blot analysis for endogenous LC3-I and LC3-II as well as p62. Induction of autophagy with Rap and block with BafA1 for 6 hr resulted in increase of LC3II compared to DMSO in control fibroblasts, while there was no acute response observed in DRPLA patient samples. No changes in

p62 levels were evident after 6 hr acute treatment.(M and N) Analysis of the autophagy flux in control and DRPLA fibroblasts (DRPLA 17) transfected with the tandem RFP-GFP-LC3B reporter. Starvation in Hank's balanced salt solution (HBSS) medium was used to induce autophagy, BafA1 treatment to inhibit lysosomal degradation. Autophagosomes are marked by yellow signal as a result of combined RFP and GFP double fluorescence. Due to quenching of the GFP signal in acidic environment autolysosomes show RFP fluorescence only. Representative images acquired with Nikon spinning disc confocal microscope display a greater amount of autophagosomes and autolysosomes in control fibroblasts compared to DRPLA after starvation in HBSS for 3 hr (M). Quantification in (N) demonstrates a significant increase in both autophagosomes and autolysosomes in control but not in DRPLA cells after starvation. Addition of BafA1 to starvation medium resulted in a greater number of GFP+RFP+ puncta as compared to starvation only in control cells. No changes were significant in DRPLA patient fibroblasts (see also Figure S6H). Significance values in the columns show differences for fed versus starved condition and starved versus +BafA1 condition for RFP+ or GFP+RFP+ puncta. One-way ANOVA, mean ± SEM, p < 0.05, p < 0.001. Significance values between control and DRPLA cells for overall puncta are shown above the horizontal bars, two-way ANOVA p < 0.001; v1, genotype; v2,- total GFP+ and GFP+RFP+ puncta. Scale bar, 20 µm.See also Figures S3 and S4. Figure provided by CiteAb. Source: Curr Biol, PMID: 29174892.

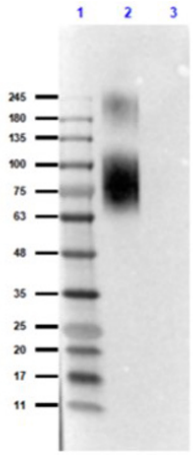

Western Blot

Western Blot of Rabbit Anti-ATG13pS318 Antibody.
Lane 1: Opal Prestained Molecular Weight Marker (p/n MB-210-0500).
Lane 2: BSA Conjugated ATG13 phospho S318 peptide - reduced [0.2µg].
Lane 3: BSA Conjugated ATG13 non-phospho S318 peptide - reduced [0.2µg].
Primary Antibody: Anti-ATG13pS318 [Rabbit] Antibody at 1.0µg/mL overnight at 2-8°C.
Secondary Antibody: Anti-Rabbit IgG [Goat] Peroxidase conjugated (p/n 611-1302) at 1:40,000 for 30mins at RT.
Block: Blocking Buffer for Fluorescent Western Blotting (p/n MB-070) for 1hr at RT.
Expected: detects the phospho S318 peptide and does not detect the NP-peptide.
Exposure: 6.1sec.

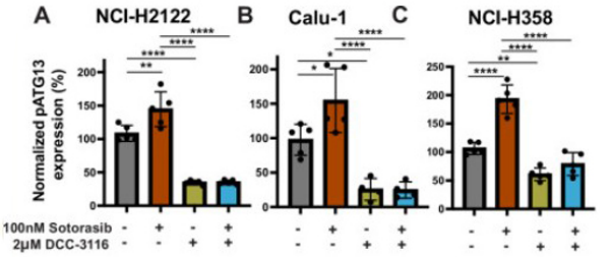

ELISA

(A–C) ELISA measurement of pS318-ATG13 signal after 16 hr of drug treatment in NCI-H2122 (A), Calu-1 (B), and NCI-H358 cell lines (C). N = 3. Statistical analysis was performed using an ordinary one-way ANOVA with Tukey's multiple comparisons test. ns = not significant, *p<0.05, ****p<0.0001. Figure 1—figure supplement 2. PMID: 39213022

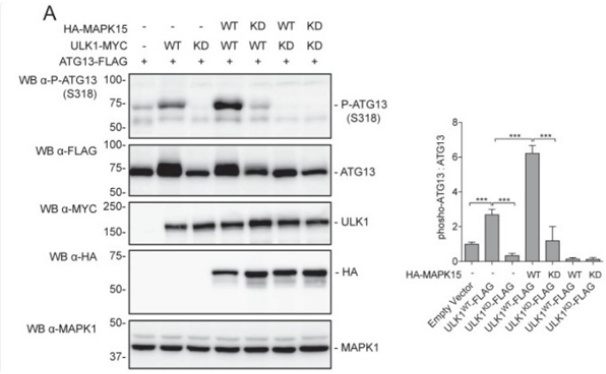

Western Blot

MAPK15 activates ULK1. A, HeLa cells were transfected with plasmid encoding for ATG13-FLAG in combination with HA-MAPK15WT, HA-MAPK15KD, ULK1WT-MYC, ULK1KD-MYC, or the empty vector. After 24 h, total lysates were analyzed by Western blot (WB) analysis (left panel). ATG13 was analyzed for phosphorylation levels [anti-phospho-ATG13 Ser318 (p/n 600-401-C49); anti-ATG13 (p/n 600-401-C50)], and scores were plotted on the graph (right panel, n = 3). Fig 2. PMID: 30131341

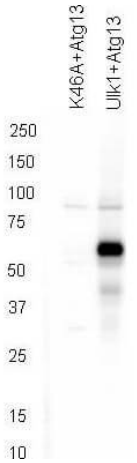

Western Blot
Western blot using Rockland's affinity purified anti-ATG13 pS318 antibody shows detection of phosphorylated ATG13 in 293T cells engineered to coexpress Ulk1 and Atg13 (Ulk1 + Atg13). In the left lane was loaded kinase-dead hypophosphorylated Ulk1-K46A mutant + ATG13. The right lane contains the 293T Ulk1 + ATG13 lysate and shows detection at approximately 57 kDa. The antibody was purified and resolved by SDS-PAGE, then transferred to nitrocellulose membrane. The membrane was blocked with 5% Blotto (p/n B501-0500) and probed with the primary antibody at 1µg/mL overnight at 4°C. After washing, the membrane was probed with Goat Anti-Rabbit HRP secondary 1:5000 in detection buffer (p/n MB-070) for 45 minutes at room temperature. In collaboration with Charles Dorsey at Eli Lilly, Indianapolis, IN and John Cleveland at Scripps, Jupiter, FL.

References

- Cong Y et al. Influenza A virus subverts the LC3-pericentrin dynein adaptor complex for host cytoplasm entry. *Sci Adv.* (2025)
- Ghazi PC et al. Inhibition of ULK1/2 and KRASG12C controls tumor growth in preclinical models of lung cancer. *Elife.* (2024)
- Ikeda R et a. Phosphorylation of phase-separated p62 bodies by ULK1 activates a redox-independent stress response. *EMBO J.* (2023)
- Brobbey C et al. Autophagy dictates sensitivity to PRMT5 inhibitor in breast cancer. *Sci Rep.* (2023)
- Kallergi E et al. Profiling of purified autophagic vesicle degradome in the maturing and aging brain. *Neuron.* (2023)
- Zhang Y et al. M6 A demethylase fat mass and obesity-associated protein regulates cisplatin resistance of gastric cancer by modulating autophagy activation through ULK1. *Cancer Sci.* (2022)
- Ktena N et al. Autophagic degradation of CNS myelin maintains axon integrity. *Cell Stress.* (2022)
- Tsang T et al. BRAFV600E-Driven Lung Adenocarcinoma Requires Copper to Sustain Autophagic Signaling and Processing. *Mol Cancer Res.* (2022)
- Kallergi E et al. Dendritic autophagy degrades postsynaptic proteins and is required for long-term synaptic depression in mice. *Nat Commun.* (2022)
- Martínez-Martínez, E et al. A Dual-Acting Nitric Oxide Donor and Phosphodiesterase 5 Inhibitor Activates Autophagy in Primary Skin Fibroblasts. *International Journal of Molecular Sciences* (2022)
- Munson, MJ et al. GAK and PRKCD are positive regulators of PRKN-independent mitophagy. *Nature Communications* (2021)
- Carinci M et al. TFG binds LC3C to regulate ULK1 localization and autophagosome formation. *EMBO J.* (2021)

- Mercer TJ et al. Phosphoproteomic identification of ULK substrates reveals VPS15-dependent ULK/VPS34 interplay in the regulation of autophagy. *EMBO J.* (2021)
- Humbert M et al. Reducing FASN expression sensitizes acute myeloid leukemia cells to differentiation therapy. *Cell Death Differ.* (2021)
- Ryu HY et al. GSK3B induces autophagy by phosphorylating ULK1. *Exp Mol Med.* (2021)
- Thayer, JA et al. The PARK10 gene USP24 is a negative regulator of autophagy and ULK1 protein stability. *Autophagy* (2020)
- Ren, H et al. Design, Synthesis, and Characterization of an Orally Active Dual-Specific ULK1/2 Autophagy Inhibitor that Synergizes with the PARP Inhibitor Olaparib for the Treatment of Triple-Negative Breast Cancer. *Journal of Medicinal Chemistry* (2020)
- Tsang T et al. Copper is an essential regulator of the autophagic kinases ULK1/2 to drive lung adenocarcinoma. *Nat Cell Biol.* (2020)
- Wirth M et al. Autophagy Pathway Mapping to Elucidate the Function of Novel Autophagy Regulators Identified by High-Throughput Screening. *Methods Mol Biol.* (2019)
- Luhr M et al. The kinase PERK and the transcription factor ATF4 play distinct and essential roles in autophagy resulting from tunicamycin-induced ER stress. *J Biol Chem.* (2019)
- Wang B et al. ULK1 and ULK2 regulate stress granule disassembly through phosphorylation and activation of VCP/p97. *Mol Cell.* (2019)
- Fuqua, JD et al. ULK2 is essential for degradation of ubiquitinated protein aggregates and homeostasis in skeletal muscle. *Faseb Journal : Official Publication of the Federation of American Societies for Experimental Biology* (2019)
- Izumi et al. Recycling endosomal CD133 functions as an inhibitor of autophagy at the pericentrosomal region. *Scientific Reports* (2019)
- Jia R et al. Negative regulation of autophagy by UBA6-BIRC6-mediated ubiquitination of LC3. *ELife* (2019)
- Wallot-Hieke N et al. Systematic analysis of ATG13 domain requirements for autophagy induction. *Autophagy.* (2018)
- Colecchia D et al. MAPK15 is part of the ULK complex and controls its activity to regulate early phases of the autophagic process. *J Biol Chem.* (2018)
- Jeong, YT et al. The ULK1-FBXW5-SEC23B nexus controls autophagy. *ELife* (2018)
- Wang et al. Phosphorylation of ULK1 affects autophagosome fusion and links chaperone-mediated autophagy to macroautophagy. *Nature Communications* (2018)
- Baron, O et al. Stall in Canonical Autophagy-Lysosome Pathways Prompts Nucleophagy-Based Nuclear Breakdown in Neurodegeneration. *Current Biology : Cb* (2017)
- Jung J et al. Multiplex image-based autophagy RNAi screening identifies SMCR8 as ULK1 kinase activity and gene expression regulator. *Elife* (2017)
- Xie Y et al. Assessment of posttranslational modifications of ATG proteins. *Methods Enzymol.* (2017)
- Stork B et al Study of ULK1 Catalytic Activity and Its Regulation. *Methods Enzymol.* (2017)

- Puente et al. Nutrient-regulated Phosphorylation of ATG13 Inhibits Starvation-induced Autophagy. *Journal of Biological Chemistry* (2016)
- View More ...

Disclaimer